

Trigonal-to-monoclinic structural transition in TiSe_2 due to a combined condensation of $q = (\frac{1}{2}, 0, 0)$ and $(\frac{1}{2}, 0, \frac{1}{2})$ phonon instabilities

Alaska Subedi 

CPHT, CNRS, Ecole Polytechnique, IP Paris, F-91128 Palaiseau, France

 (Received 26 July 2021; revised 7 December 2021; accepted 6 January 2022; published 14 January 2022)

I present first principles calculations of the phonon dispersions of TiSe_2 in the $P\bar{3}c1$ phase, which is the currently accepted low-temperature structure of this material. They show weak instabilities in the acoustic branches in the out-of-plane direction, suggesting that this phase may not be the true ground state. To find the lowest energy structure, I study the energetics of all possible distorted structures corresponding to the isotropy subgroups of $P\bar{3}m1$ for the M_1^- and L_1^- phonon instabilities present in this high-temperature phase at $q = (\frac{1}{2}, 0, 0)$ and $(\frac{1}{2}, 0, \frac{1}{2})$, respectively. I am able to stabilize ten different structures that are lower in energy relative to the parent $P\bar{3}m1$ phase, including two monoclinic structures more energetically stable than the $P\bar{3}c1$ phase. The lowest energy structure has the space group $C2$ with the order parameter $M_1^-(a, 0, 0) + L_1^-(0, b, b)$. This structure lacks inversion symmetry, and its primitive unit cell has 12 atoms.

DOI: [10.1103/PhysRevMaterials.6.014602](https://doi.org/10.1103/PhysRevMaterials.6.014602)

I. INTRODUCTION

The structural transition near 200 K in $1T$ - TiSe_2 has been frequently studied since its three-directional superlattice was reported by Di Salvo *et al.* in 1976 [1]. A phonon softening at the wave vector $(\frac{1}{2}, 0, \frac{1}{2})$ in the parent phase of this material has been unambiguously identified [2,3], but the microscopic mechanism underlying this charge density wave (CDW) transition is still being debated. The parent phase of TiSe_2 is either a semimetal or a semiconductor with a low carrier concentration [1,4–16], which precludes an explanation based on Fermi surface nesting. Hence, other mechanisms such as excitonic condensation [17–21], Jahn-Teller effect [22–24], incipient antiferroelectricity [25,26], electron-phonon coupling [27–30], or some combination thereof [31–35] has been invoked to explain this transition.

The high-temperature phase of TiSe_2 occurs in a trigonal structure with the space group $P\bar{3}m1$ [36,37]. This structure is composed of hexagonal layers of Ti sandwiched between two hexagonal layers of Se such that the Ti ions are situated inside Se octahedra. Each layer has three twofold rotational axes and three mirror planes along and perpendicular, respectively, to the three chains forming the hexagonal lattice. The low-temperature phase has been reported to form a $2 \times 2 \times 2$ superlattice with the space group $P\bar{3}c1$ [38]. In this structure, all the three twofold rotational symmetries present in each layer are broken. However, the presence of a glide plane restores the twofold rotational symmetries in the full lattice.

There are experimental indications that further rotational, mirror, and inversion symmetries are broken in the low-temperature phase. Ishioka *et al.* have claimed that the CDW phase in this material is chiral based on their scanning tunneling microscopy (STM) experiments [39,40]. Such a chiral phase has been theoretically understood as a form of orbital ordering [41–43], and there are experimental evidences

supporting this claim [44–46]. However, more recent STM experiments have questioned this interpretation and suggest that the CDW phase is achiral [47,48]. In the midst of this debate [49–51], Xu *et al.* have reported the measurements of circular photogalvanic effect current that suggests the presence of a low-symmetry structure without inversion symmetry below 174 K [52]. But this gyrotropic phase has been argued to occur only in the photoexcited state [53].

The electronic properties of TiSe_2 and the structural instability of its high-temperature phase has been extensively studied using density functional theory (DFT) based first principles calculations [15,54–63]. However, neither the structural stability of the $P\bar{3}c1$ CDW phase nor a detailed study of all possible structures arising out of the phonon instabilities present in the parent phase has been investigated using DFT calculations. In particular, the energetics of the low-symmetry structures resulting from a combined condensation of the phonon instabilities at M $(\frac{1}{2}, 0, 0)$ and L $(\frac{1}{2}, 0, \frac{1}{2})$ has not been explored. A theoretical study examining these aspects would be helpful in answering whether a structure with broken inversion symmetry is the true ground state of pure TiSe_2 or it is induced by external stimuli such as defects and photoexcitations.

In this paper, I present the calculated phonon dispersions of the $2 \times 2 \times 2$ $P\bar{3}c1$ phase, which show acoustic branches with weak instabilities in the out-of-plane direction. This suggests that the $P\bar{3}c1$ structure may not be the true ground state of this material. To find the lowest energy structure, I generated all possible distortions corresponding to the isotropy subgroups that can arise due to the phonon instabilities at the M and L points present in the parent $P\bar{3}m1$ phase of the material. After full structural relaxations minimizing both the forces and stresses, I was able to stabilize ten different structures that are lower in energy than the parent $P\bar{3}m1$ phase. These include two monoclinic structures that are more energetically stable

than the $P\bar{3}c1$ phase. The lowest energy structure has the space group $C2$ with the order parameter $M_1^-(a, 0, 0) + L_1^-(0, b, b)$. This structure has no inversion symmetry, and its primitive unit cell has 12 atoms.

II. COMPUTATIONAL APPROACH

The phonon dispersions and structural relaxation calculations presented here were performed using the pseudopotential-based QUANTUM ESPRESSO package [64]. I used the pseudopotentials generated by Dal Corso [65] and energy cutoffs of 60 and 600 Ry for the basis-set and charge density expansions, respectively. The calculations were performed using the optB88-vdW exchange-correlation functional that accurately treats the van der Waals interaction [66]. In the phonon calculations, $24 \times 24 \times 12$ and $12 \times 12 \times 6$ k -point grids were used for the Brillouin zone integration in the $P\bar{3}m1$ and $P\bar{3}c1$ phases, respectively. Dynamical matrices were calculated on a $8 \times 8 \times 4$ grid for the $P\bar{3}m1$ phase and a $4 \times 4 \times 4$ grid for the $P\bar{3}c1$ phase using density functional perturbation theory [67], and Fourier interpolation was used to obtain the phonon dispersions. I used the ISOTROPY package to enumerate all the order parameters that are possible due to the unstable phonon modes M_1^- and L_1^- of the parent phase [68]. Structural relaxation calculations of the structures corresponding to different isotropy subgroups were performed on $2 \times 2 \times 2$ supercells using a $20 \times 20 \times 10$ k -point grid. I checked the relative energy orderings of the two lowest energy structures using a $24 \times 24 \times 12$ k -point grid and 85 Ry basis-set cutoff. A 0.01 Ry Marzari-Vanderbilt smearing was used in all the calculations.

A recent study has shown that hybrid functionals accurately describe the insulating electronic structure of TiSe_2 [62]. Furthermore, they also lead to an enhanced energy gain for the distorted $P\bar{3}c1$ phase relative to the undistorted $P\bar{3}m1$ phase. Using the HSE06+D2 functional [69,70], I fully relaxed and calculated the total energy of the lowest-energy optB88-vdW structure and compared it with that of the $P\bar{3}m1$ and $P\bar{3}c1$ phases. Hybrid functional calculations on $2 \times 2 \times 2$ supercells of TiSe_2 are computationally heavy. So only the main result of the paper was checked using the HSE06+D2 functional. These calculations were performed using the pseudopotential-based VASP code [71]. A basis-set cutoff of 320 eV and $6 \times 6 \times 3$ k point were used in these calculations.

I made extensive use of the FINDSYM [72], AMPLIMODES [73], SPGLIB [74], and PHONOPY [75] packages in the symmetry analysis of the relaxed structures. A previous study has shown that the spin-orbit interaction does not modify the structural instability of this material [62], so it was neglected in all the calculations presented in this paper.

III. RESULTS AND DISCUSSION

The calculated optB88-vdW phonon dispersions of the fully relaxed TiSe_2 in the parent $P\bar{3}m1$ structure is shown in Fig. 1. They agree well with the previous calculations when either the experimental lattice parameters or the theoretical ones close to the experimental values are used [57,62].

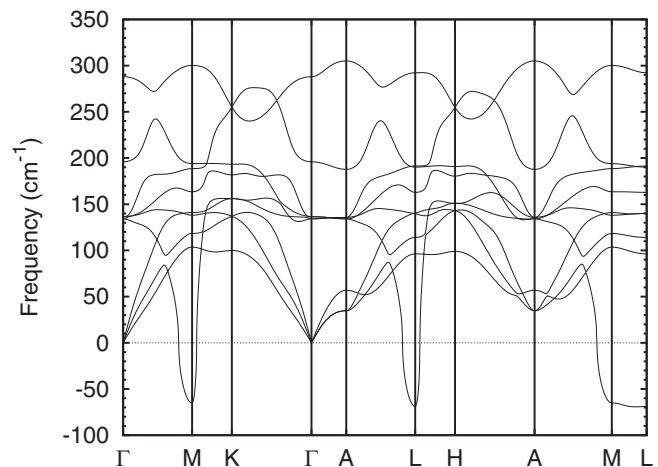


FIG. 1. Calculated phonon dispersions of TiSe_2 in the parent $P\bar{3}m1$ phase calculated using the optB88-vdW functional. The high-symmetry points are Γ (0, 0, 0), M ($\frac{1}{2}$, 0, 0), K ($\frac{1}{3}$, $\frac{1}{3}$, 0), A (0, 0, $\frac{1}{2}$), L ($\frac{1}{2}$, 0, $\frac{1}{2}$), and H ($\frac{1}{3}$, $\frac{1}{3}$, $\frac{1}{2}$) in terms of the reciprocal lattice vectors.

The calculated values of the A_g 196 cm^{-1} and highest-frequency E_u 135 cm^{-1} modes also compare well with the experimental values of A_g 200 cm^{-1} [76] and E_u 137 cm^{-1} [77]. There is a phonon branch that is unstable along the path M - L . Both M $\{(0, \frac{1}{2}, 0), (\frac{1}{2}, 0, 0), (\frac{1}{2}, \frac{1}{2}, 0)\}$ and L $\{(0, \frac{1}{2}, \frac{1}{2}), (\frac{1}{2}, 0, \frac{1}{2}), (\frac{1}{2}, \frac{1}{2}, \frac{1}{2})\}$ have three elements in their star. Hence, even though the unstable branch is nondegenerate, several low-symmetry structures are possible due to these instabilities. The instability at L is slightly stronger than at M , and the low-temperature CDW phase of this material has been understood to form due to the simultaneous condensation at the three wave vectors belonging to L [1]. Indeed, Bianco *et al.* have performed a detailed DFT-based theoretical study and found that the energy gain due to the triple- q condensation at L is larger than the triple- q condensation at M as well as single- q condensations at L and M [61]. I also note that calculations using the fully relaxed lattice parameters obtained within the local density approximation (LDA) do not show any structural instability because LDA underestimates the volume of the unit cell [78].

Although the structural instability of the high-temperature phase of TiSe_2 has been extensively studied using DFT-based calculations [3,57,61,62], the relative energetic stability of all possible structures arising due to the instabilities at M and L has yet to be investigated. In fact, the structural stability of the currently accepted low-temperature triple- q $P\bar{3}c1$ phase has not been confirmed theoretically despite there being experimental evidences that the low-temperature structure has a symmetry lower than trigonal [39,52]. I calculated the phonon dispersions of the fully relaxed $P\bar{3}c1$ phase, which is shown in Fig. 2. I find that all the optical phonon branches are stable. However, the acoustic branches show weak instabilities in the out-of-plane $(0, 0, q_z)$ direction. The instabilities occur for $q_z < \frac{1}{6}$, which is not in the $4 \times 4 \times 4$ grid used to calculate the dynamical matrices. To confirm the presence of the instabilities, I calculated the dynamical matrices at $q_z = \frac{1}{16}$ and $\frac{1}{24}$, which yielded three modes with imaginary frequencies. This

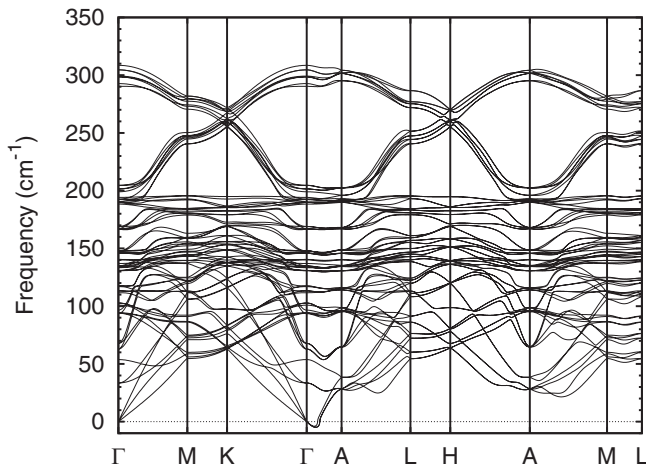


FIG. 2. Calculated phonon dispersions of TiSe_2 in the $L_1^-(a, a, a) P\bar{3}c1$ phase calculated using the optB88-vdW functional. The acoustic branches are unstable in the out-of-plane direction Γ -A.

suggests that the currently accepted low-temperature $P\bar{3}c1$ structure may not be the true ground state of this material.

The unstable phonon branch in the parent $P\bar{3}m1$ phase has the representations M_1^- and L_1^- at M and L , respectively. I used the ISOTROPY package to determine all the isotropy subgroups and order parameters that are possible due to these two unstable phonons, which are listed in Table I. I then used the calculated phonon displacement vectors of the unstable modes to generate all 26 possible distortions corresponding to the isotropy subgroups on $2 \times 2 \times 2$ supercells of the high-temperature parent phase and fully relaxed these structures by minimizing both the atomic forces and lattice stresses.

I was able to stabilize ten different structures characterized by distinct order parameters that have their calculated energies lower than that of the high-temperature $P\bar{3}m1$ phase. These include the single- and triple- q structures due to the M_1^- and L_1^- instabilities discussed previously by Bianco *et al.* [61]. Interestingly, there are three distinct structures belonging to the same isotropy subgroup $C2/c$ and two structures with the subgroup $C2/m$. The calculated total energies of all these structures are given in Table I. The energy gains due to structural distortions are small, consistent with previous results [61]. The $P\bar{3}c1$ structure is only -1.184 meV per formula unit (meV/f.u.) lower than the parent $P\bar{3}m1$ phase. I find two more structures lower in energy than the $P\bar{3}c1$ structure. They have space groups $C2/c$ and $C2$ with energies -1.188 and -1.192 meV/f.u. relative to the parent phase, respectively.

Recent calculations using hybrid functionals show that the gain in energy due to the $P\bar{3}c1$ distortions are enhanced relative to the undistorted $P\bar{3}m1$ phase when the nonlocal exchange interaction is taken into account [62]. I checked the main finding of this paper by performing full relaxations of the $P\bar{3}m1$, $P\bar{3}c1$, and $C2$ phases using the HSE06 functional in combination with Grimme's semiempirical treatment of the van der Waals interaction. I find that the energy gain of the $P\bar{3}c1$ phase relative to the $P\bar{3}m1$ phase increases to 4.7475 meV/f.u., which is almost a fourfold increase compared to the optB88-vdW value. The gain of the $C2$ phase relative to the $P\bar{3}m1$ phase increases to 4.7563 meV/f.u. The $C2$

TABLE I. Isotropy subgroups of $P\bar{3}m1$ for the representations L_1^- and M_1^- , and the corresponding six-dimensional order parameters in the subspace spanned by the stars of $M\{(0, \frac{1}{2}, 0), (\frac{1}{2}, 0, 0), (\frac{1}{2}, \frac{1}{2}, 0)\}$ and $L\{(0, \frac{1}{2}, \frac{1}{2}), (\frac{1}{2}, 0, \frac{1}{2}), (\frac{1}{2}, \frac{1}{2}, \frac{1}{2})\}$. Total energies of the structures corresponding to these order parameters after full structural relaxations minimizing the atomic forces and lattice stresses are given in the units of meV per formula unit relative to the parent $P\bar{3}m1$ phase. Not all distortions could be stabilized.

Space group (No.)	M_1^-	L_1^-	Energy (meV/f.u.)
$P\bar{3}m1$ (164)	(0,0,0)	(0,0,0)	0.000
$P2/c$ (13)	(a, 0, 0)	(0,0,0)	-0.726
$C2/c$ (15)	(0,0,0)	(a, 0, 0)	-0.755
$C2/m$ (12)	(a, a, 0)	(0,0,0)	-1.004
$P\bar{1}$ (2)	(a, 0, 0)	(0, b, 0)	-1.031
$C2/m$ (12)	(0,0,0)	(a, a, 0)	-1.046
$P321$ (150)	(a, a, a)	(0,0,0)	-1.136
$C2/c$ (15)	(a, a, 0)	(0, 0, b)	-1.170
$P\bar{3}c1$ (165)	(0,0,0)	(a, a, a)	-1.184
$C2/c$ (15)	(0,0,0)	(a, a, b)	-1.188
$C2$ (5)	(a, 0, 0)	(0, b, b)	-1.192
$P\bar{1}$ (2)	(a, b, 0)	(0,0,0)	
$C2$ (5)	(a, a, b)	(0,0,0)	
$P1$ (1)	(a, b, c)	(0,0,0)	
$P\bar{1}$ (2)	(0,0,0)	(a, b, 0)	
$P\bar{1}$ (2)	(0,0,0)	(a, b, c)	
$P2/c$ (13)	(a, 0, 0)	(b, 0, 0)	
$P\bar{1}$ (2)	(a, b, 0)	(0, 0, c)	
$C2/m$ (12)	(a, a, 0)	(b, b, 0)	
$C2/c$ (15)	(a, a, 0)	(b, -b, 0)	
$C2$ (5)	(a, a, b)	(c, -c, 0)	
$P1$ (1)	(a, 0, 0)	(0, b, c)	
$P\bar{1}$ (2)	(a, b, 0)	(c, d, 0)	
$P321$ (150)	(a, a, a)	(b, b, b)	
Cc (9)	(a, a, 0)	(b, -b, -c)	
$C2$ (5)	(a, a, b)	(c, c, d)	
$P1$ (1)	(a, b, c)	(d, e, f)	

phase is still the energetically most favored phase, and its energy gain relative to the $P\bar{3}c1$ phase is now increased to 0.0088 meV/f.u. compared to 0.004 meV/f.u. obtained using the optB88-vdW functional. The increase in calculated energy gain due to structural distortions using the HSE06+D2 functional suggests that electronic interactions beyond those described by the optB88-vdW functional play an important role in the structural transition of this material, as suggested by Hellgren *et al.* [62].

Figure 3 shows the $z = 0$ and $\frac{1}{2}$ hexagonal Ti layers in the parent $P\bar{3}m1$ and the three lowest energy structures with space groups $P\bar{3}c1$, $C2/c$, and $C2$. Their full structural parameters are given in Tables II, III, IV, and V, respectively. In the $P\bar{3}m1$ phase, all the Ti-Ti distances in the Ti triangles are equal, and the calculated value of 3.5548 \AA is in good agreement with the experimentally determined one of 3.540 \AA [37]. Each element of the unstable mode at both M and L causes nearest-neighbor antiparallel slidings within one set of the three intersecting Ti chains that form the hexagonal lattice [1,61]. This breaks the twofold rotational symmetries the lie along the two other sets of Ti chains. The $P\bar{3}c1$ phase has the order parameter

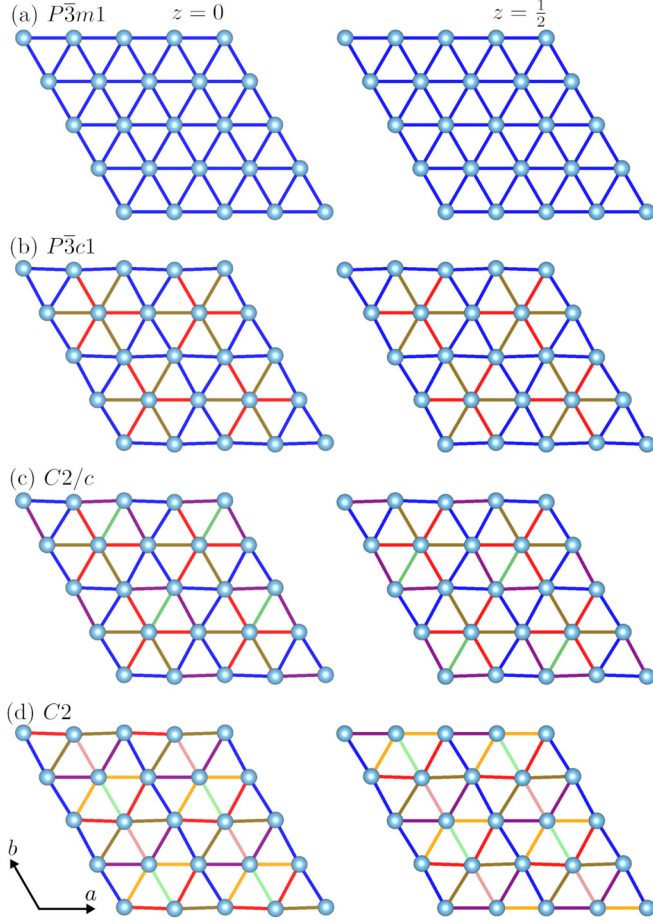


FIG. 3. Ti hexagonal layers present in the (a) parent $P\bar{3}m1$, (b) $L_1^-(a, a, a)$ $P\bar{3}c1$, (c) $L_1^-(a, a, b)$ $C2/c$, and (d) $M_1^-(a, 0, 0) + L_1^-(0, b, b)$ $C2$ phases of TiSe_2 . There are one, three, five, and seven nonequivalent Ti-Ti distances in the four phases, respectively, which are indicated by different colors. For each phase, the left and right columns show the $z = 0$ and $\frac{1}{2}$ layers, respectively, of the $2 \times 2 \times 2$ supercell used in the full structural relaxations.

$L_1^-(a, a, a)$ and involves simultaneous condensation of the unstable mode at all three wave vectors in the star of L with equal magnitudes. There are three nonequivalent Ti-Ti distances in this phase. The smallest calculated Ti-Ti distance is 0.068 Å shorter than the one in the parent phase, which is in reasonable agreement with the experimental value of 0.08 Å [1]. Although all the twofold rotational symmetries are broken within the hexagonal layers in this phase, the presence of a c glide plane restores the broken symmetries in the full

TABLE II. Calculated atomic coordinates of TiSe_2 in the parent $P\bar{3}m1$ phase obtained using the optb88-vdw functional. Calculated lattice parameters are $a = b = 3.55475$, $c = 6.080271$ Å, $\alpha = \beta = 90^\circ$, and $\gamma = 120^\circ$.

Atom	Site	x	y	z
Ti	$1a$	0	0	0
Se	$2d$	$1/3$	$2/3$	0.25438

TABLE III. Calculated atomic coordinates of TiSe_2 in the $L_1^-(a, a, a)$ $P\bar{3}c1$ phase obtained using the optb88-vdw functional. Calculated lattice parameters are $a = b = 7.11167$, $c = 12.17568$ Å, $\alpha = \beta = 90^\circ$, and $\gamma = 120^\circ$.

Atom	Site	x	y	z
Ti1	$2a$	0	0	$1/4$
Ti2	$6f$	0.50943	0	$1/4$
Se1	$4d$	$1/3$	$2/3$	0.62316
Se2	$12g$	0.66700	0.83055	0.87735

three-dimensional lattice. This glide plane relates the $z = 0$ and $\frac{1}{2}$ Ti layers, which is demonstrated in Fig. 3(b).

The $C2/c$ phase that is lower in energy than the $P\bar{3}c1$ phase has the order parameter $L_1^-(a, a, b)$. Since a component of the order parameter is different along one direction, two additional Ti-Ti distances become nonequivalent, for a total of five different bond lengths in the hexagonal layer. This additionally breaks the threefold rotational axis perpendicular to the hexagonal plane. However, changes in the Ti-Ti distances due to this monoclinic distortion is less than 2.0×10^{-4} Å relative to the $P\bar{3}c1$ phase, and the monoclinic angle β deviates from 90° by only 0.0016° . The $z = 0$ and $\frac{1}{2}$ layers in this phase are again related by the c glide plane, as can be seen in Fig. 3(c).

The lowest-energy $C2$ phase involves condensation of both M_1^- and L_1^- instabilities and has the order parameter $M_1^-(a, 0, 0) + L_1^-(0, b, b)$. Two more Ti-Ti distances become nonequivalent, and this phase lacks the mirror as well as inversion symmetries present in the $C2/c$ phase. However, this phase possesses a twofold rotation axis that passes through the pink and green bonds along the b direction in Fig. 3(d). Additionally, the $z = 0$ and $\frac{1}{2}$ layers are related by a shift along the b axis. The changes in the Ti-Ti distances in this structure are up to 1.1×10^{-3} Å relative to the $P\bar{3}c1$ phase, which is larger than that calculated for the $C2/c$ structure. Unlike the $P\bar{3}c1$ and $C2/m$ structures, the $C2$ structure has 12 atoms in its primitive unit cell.

The calculated differences in the Ti-Ti bond distances between the three distorted phases $P\bar{3}c1$, $C2/c$, and $C2$ are tiny, which may be one of the reasons that the monoclinic phase is not fully resolved in diffraction experiments. Figure 4 shows the calculated phonon frequencies of the $P\bar{3}m1$, $P\bar{3}c1$, $C2/c$,

TABLE IV. Calculated atomic coordinates of TiSe_2 in the $L_1^-(a, a, b)$ $C2/m$ phase obtained using the optb88-vdw functional. Calculated lattice parameters are $a = 12.31768$, $b = 7.11156$, $c = 12.17613$ Å, $\alpha = 90^\circ$, $\beta = 90.00156^\circ$, and $\gamma = 90^\circ$.

Atom	Site	x	y	z
Ti1	$4e$	0	0.00943	$1/4$
Ti2	$4e$	0	0.50001	$1/4$
Ti3	$8f$	0.25471	0.24528	0.25000
Se1	$8f$	-0.08177	0.24877	0.37735
Se2	$8f$	0.66650	0.00296	0.37735
Se3	$8f$	0.16667	0.00000	0.37684
Se4	$8f$	0.41528	0.24827	0.37735

TABLE V. Calculated atomic coordinates of TiSe_2 in the $M_1^-(a, 0, 0) + L_1^-(0, b, b)$ $C2$ phase obtained using the optb88-vdW functional. Calculated lattice parameters are $a = 12.17894$, $b = 7.11183$, $c = 8.66017$ Å, $\alpha = 90^\circ$, $\beta = 134.67258^\circ$, and $\gamma = 90^\circ$.

Atom	Site	x	y	z
Ti1	2b	0	0.49045	1/2
Ti2	2b	0	0.00005	1/2
Ti3	4c	0.74521	0.25469	-0.00960
Se1	4c	0.79384	0.49698	0.83295
Se2	4c	0.54259	0.25178	0.33048
Se3	4c	0.79347	0.00000	0.83333
Se4	4c	0.04560	0.25121	0.33650

and $C2$ phases of TiSe_2 at the Brillouin zone center obtained using the optB88-vdW functional for the fully relaxed primitive unit cell of the respective phases. The phonon spectra at the zone center are both quantitatively and qualitatively different depending upon the number of atoms present in the primitive unit cell. In particular, the lowest-lying optical phonon mode of the currently accepted low-temperature $P\bar{3}c1$ phase has a frequency of 33 cm^{-1} , whereas that of the proposed lowest-energy $C2$ phase has a frequency of 56 cm^{-1} . Therefore, the measurement of the lowest-lying optical phonon mode below the structural transition temperature may help in verifying whether the proposed $C2$ phase is the ground state structure of this material.

IV. SUMMARY AND CONCLUSIONS

In summary, I have presented the phonon dispersions of the $2 \times 2 \times 2$ $P\bar{3}c1$ phase of TiSe_2 , which is the currently accepted low-temperature structure of this material. They show weak instabilities in the acoustic branches, suggesting that this phase might not be the ground state. To find the lowest energy structure, I studied the energetics of all possible structures corresponding to the isotropy subgroups due to the M_1^- and

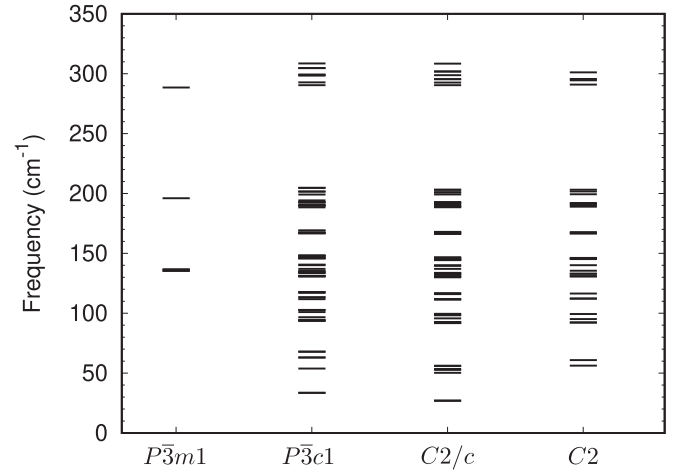


FIG. 4. Calculated phonon frequencies of the $P\bar{3}m1$, $P\bar{3}c1$, $C2/c$, and $C2$ phases of TiSe_2 at the Brillouin zone center obtained using the optB88-vdW functional. The phonons are calculated for the primitive unit cells of the respective phases.

L_1^- phonon instabilities present in the parent $P\bar{3}m1$ phase. The structure with the lowest energy has the space group $C2$ and order parameter $M_1^-(a, 0, 0) + L_1^-(0, b, b)$. The primitive unit cell of this phase has 12 atoms, and it lacks inversion symmetry. The calculated frequencies of the lowest-lying optical phonon modes at the Brillouin zone center are 33 and 56 cm^{-1} , respectively, for the $P\bar{3}c1$ and $C2$ phases. Hence, the measurement of the zone center phonon spectra may be useful in discriminating between the two distorted phases.

ACKNOWLEDGMENTS

I am grateful to B. J. Kim for helpful discussions. This work was supported by Agence Nationale de la Recherche under Grant No. ANR-19-CE30-0004. The computational resources were provided by GENCI-CINES (Grant No. A0090911099) and the Swiss National Supercomputing Center (Grant No. s820).

- [1] F. J. Di Salvo, D. E. Moncton, and J. V. Waszczak, *Phys. Rev. B* **14**, 4321 (1976).
- [2] M. Holt, P. Zschack, H. Hong, M. Y. Chou, and T.-C. Chiang, *Phys. Rev. Lett.* **86**, 3799 (2001).
- [3] F. Weber, S. Rosenkranz, J.-P. Castellan, R. Osborn, G. Karapetrov, R. Hott, R. Heid, K.-P. Bohnen, and A. Alatas, *Phys. Rev. Lett.* **107**, 266401 (2011).
- [4] N. G. Stoffel, S. D. Kevan, and N. V. Smith, *Phys. Rev. B* **31**, 8049 (1985).
- [5] O. Anderson, R. Mancke, and M. Skibowski, *Phys. Rev. Lett.* **55**, 2188 (1985).
- [6] Th. Pillo, J. Hayoz, H. Berger, F. Lévy, L. Schlapbach, and P. Aebi, *Phys. Rev. B* **61**, 16213 (2000).
- [7] T. E. Kidd, T. Miller, M. Y. Chou, and T.-C. Chiang, *Phys. Rev. Lett.* **88**, 226402 (2002).
- [8] K. Rossnagel, L. Kipp, and M. Skibowski, *Phys. Rev. B* **65**, 235101 (2002).
- [9] X. Y. Cui, H. Negishi, S. G. Titova, K. Shimada, A. Ohnishi, M. Higashiguchi, Y. Miura, S. Hino, A. M. Jahir, A. Titov, H. Bidadi, S. Negishi, H. Namatame, M. Taniguchi, and M. Sasaki, *Phys. Rev. B* **73**, 085111 (2006).
- [10] D. Qian, D. Hsieh, L. Wray, E. Morosan, N. L. Wang, Y. Xia, R. J. Cava, and M. Z. Hasan, *Phys. Rev. Lett.* **98**, 117007 (2007).
- [11] G. Li, W. Z. Hu, D. Qian, D. Hsieh, M. Z. Hasan, E. Morosan, R. J. Cava, and N. L. Wang, *Phys. Rev. Lett.* **99**, 027404 (2007).
- [12] H. Cercellier, C. Monney, F. Clerc, C. Battaglia, L. Despont, M. G. Garnier, H. Beck, P. Aebi, L. Patthey, H. Berger, and L. Forró, *Phys. Rev. Lett.* **99**, 146403 (2007).
- [13] J. C. E. Rasch, T. Stemmler, B. Müller, L. Dudy, and R. Mancke, *Phys. Rev. Lett.* **101**, 237602 (2008).
- [14] T. Rohwer, S. Hellmann, M. Wiesenmayer, C. Sohrt, A. Stange, B. Slomski, A. Carr, Y. Liu, L. M. Avila, M. Kallane, S. Mathias, L. Kipp, K. Rossnagel, and M. Bauer, *Nature (London)* **471**, 490 (2011).

- [15] P. Chen, Y.-H. Chan, X.-Y. Fang, S.-K. Mo, Z. Hussain, A.-V. Fedorov, M. Y. Chou, and T.-C. Chiang, *Sci. Rep.* **6**, 37910 (2016).
- [16] M.-L. Mottas, T. Jaouen, B. Hildebrand, M. Rumo, F. Vanini, E. Razzoli, E. Giannini, C. Barreateau, D. R. Bowler, C. Monney, H. Beck, and P. Aebi, *Phys. Rev. B* **99**, 155103 (2019).
- [17] J. A. Wilson, *Solid State Commun.* **22**, 551 (1977).
- [18] C. Monney, H. Cercellier, F. Clerc, C. Battaglia, E. F. Schwier, C. Didiot, M. G. Garnier, H. Beck, P. Aebi, H. Berger, L. Forró, and L. Patthey, *Phys. Rev. B* **79**, 045116 (2009).
- [19] E. Möhr-Vorobeva, S. L. Johnson, P. Beaud, U. Staub, R. De Souza, C. Milne, G. Ingold, J. Demsar, H. Schaefer, and A. Titov, *Phys. Rev. Lett.* **107**, 036403 (2011).
- [20] M. M. May, C. Brabetz, C. Janowitz, and R. Manzke, *Phys. Rev. Lett.* **107**, 176405 (2011).
- [21] A. Kogar, M. S. Rak, S. Vig, A. A. Husain, F. Flicker, Y. I. Joe, L. Venema, G. J. MacDougall, T. C. Chiang, E. Fradkin, J. van Wezel, and P. Abbamonte, *Science* **358**, 1314 (2017).
- [22] H. P. Hughes, *J. Phys. C: Solid State Phys.* **10**, L319 (1977).
- [23] M.-H. Whangbo and E. Canadell, *J. Am. Chem. Soc.* **114**, 9587 (1992).
- [24] A. Wegner, J. Zhao, J. Li, J. Yang, A. A. Anikin, G. Karapetrov, K. Esfarjani, D. Louca, and U. Chatterjee, *Phys. Rev. B* **101**, 195145 (2020).
- [25] R. M. White and G. Lucovsky, *Nuovo Cimento B* **38**, 280 (1977).
- [26] A. Bussmann-Holder and H. Büttner, *J. Phys.: Condens. Matter* **14**, 7973 (2002).
- [27] Y. Yoshida and K. Motizuki, *J. Phys. Soc. Jpn.* **49**, 898 (1980).
- [28] K. Motizuki, Y. Yoshida, and Y. Takaoka, *Physica B+C* **105**, 357 (1981).
- [29] K. Motizuki, N. Suzuki, Y. Yoshida, and Y. Takaoka, *Solid State Commun.* **40**, 995 (1981).
- [30] N. Suzuki, A. Yamamoto, and K. Motizuki, *J. Phys. Soc. Jpn.* **54**, 4668 (1985).
- [31] J. van Wezel, P. Nahai-Williamson, and S. Saxena, *Europhys. Lett.* **89**, 47004 (2010).
- [32] J. van Wezel, P. Nahai-Williamson, and S. S. Saxena, *Phys. Rev. B* **81**, 165109 (2010).
- [33] C. Monney, C. Battaglia, H. Cercellier, P. Aebi, and H. Beck, *Phys. Rev. Lett.* **106**, 106404 (2011).
- [34] M. Porer, U. Leierseder, J.-M. Ménard, H. Dachraoui, L. Mouchliadis, I. Perakis, U. Heinzmann, J. Demsar, K. Rossnagel, and R. Huber, *Nat. Mater.* **13**, 857 (2014).
- [35] T. Kaneko, Y. Ohta, and S. Yunoki, *Phys. Rev. B* **97**, 155131 (2018).
- [36] I. Oftedal, *Z. Phys. Chem.* **134U**, 301 (1928).
- [37] C. Riekel, *J. Solid State Chem.* **17**, 389 (1976).
- [38] J. A. Wilson, *Phys. Rev. B* **17**, 3880 (1978).
- [39] J. Ishioka, Y. H. Liu, K. Shimatake, T. Kurosawa, K. Ichimura, Y. Toda, M. Oda, and S. Tanda, *Phys. Rev. Lett.* **105**, 176401 (2010).
- [40] J. Ishioka, T. Fujii, K. Katono, K. Ichimura, T. Kurosawa, M. Oda, and S. Tanda, *Phys. Rev. B* **84**, 245125 (2011).
- [41] J. van Wezel, *Europhys. Lett.* **96**, 67011 (2011).
- [42] J. van Wezel, *Phys. Rev. B* **86**, 247101 (2012).
- [43] M. Gradhand and J. van Wezel, *Phys. Rev. B* **92**, 041111(R) (2015).
- [44] M. Iavarone, R. Di Capua, X. Zhang, M. Golalikhani, S. A. Moore, and G. Karapetrov, *Phys. Rev. B* **85**, 155103 (2012).
- [45] J.-P. Castellan, S. Rosenkranz, R. Osborn, Q. Li, K. E. Gray, X. Luo, U. Welp, G. Karapetrov, J. P. C. Ruff, and J. van Wezel, *Phys. Rev. Lett.* **110**, 196404 (2013).
- [46] Y. Peng, X. Guo, Q. Xiao, Q. Li, J. Stremper, Y. Choi, D. Yan, H. Luo, Y. Huang, S. Jia, O. Janson, P. Abbamonte, J. van den Brink, J. van Wezel, *arXiv:2105.13195*.
- [47] A. M. Novello, B. Hildebrand, A. Scarfato, C. Didiot, G. Monney, A. Ubaldini, H. Berger, D. R. Bowler, P. Aebi, and Ch. Renner, *Phys. Rev. B* **92**, 081101(R) (2015).
- [48] B. Hildebrand, T. Jaouen, M.-L. Mottas, G. Monney, C. Barreateau, E. Giannini, D. R. Bowler, and P. Aebi, *Phys. Rev. Lett.* **120**, 136404 (2018).
- [49] M. K. Lin, J. A. Hlevyack, P. Chen, R. Y. Liu, and T. C. Chiang, *Phys. Rev. Lett.* **122**, 229701 (2019).
- [50] S. Rosenkranz, R. Osborn, and J. van Wezel, *Phys. Rev. Lett.* **122**, 229702 (2019).
- [51] H. Ueda, M. Porer, J. R. L. Mardegan, S. Parchenko, N. Gurung, F. Fabrizi, M. Ramakrishnan, L. Boie, M. J. Neugebauer, B. Burganov, M. Burian, S. L. Johnson, K. Rossnagel, and U. Staub, *Phys. Rev. Research* **3**, L022003 (2021).
- [52] S.-Y. Xu, Q. Ma, Y. Gao, A. Kogar, A. Zong, A. M. Mier Valdivia, T. H. Dinh, S.-M. Huang, B. Singh, C.-H. Hsu, T.-R. Chang, J. P. C. Ruff, K. Watanabe, T. Taniguchi, H. Lin, G. Karapetrov, D. Xiao, P. Jarillo-Herrero, and N. Gedik, *Nature (London)* **578**, 545 (2020).
- [53] D. Wickramaratne, R. Schaller, G. Wiederrecht, G. Karapetrov, and I. I. Mazin, *arXiv:2010.00766*.
- [54] A. Zunger and A. J. Freeman, *Phys. Rev. B* **17**, 1839 (1978).
- [55] C. M. Fang, R. A. de Groot, and C. Haas, *Phys. Rev. B* **56**, 4455 (1997).
- [56] R. A. Jishi and H. M. Alyahyaei, *Phys. Rev. B* **78**, 144516 (2008).
- [57] M. Calandra and F. Mauri, *Phys. Rev. Lett.* **106**, 196406 (2011).
- [58] M. Cazzaniga, H. Cercellier, M. Holzmann, C. Monney, P. Aebi, G. Onida, and V. Olevano, *Phys. Rev. B* **85**, 195111 (2012).
- [59] Z. Zhu, Y. Cheng, and U. Schwingenschlögl, *Phys. Rev. B* **85**, 245133 (2012).
- [60] Z. Vydrova, E. F. Schwier, G. Monney, T. Jaouen, E. Razzoli, C. Monney, B. Hildebrand, C. Didiot, H. Berger, T. Schmitt, V. N. Strocov, F. Vanini, and P. Aebi, *Phys. Rev. B* **91**, 235129 (2015).
- [61] R. Bianco, M. Calandra, and F. Mauri, *Phys. Rev. B* **92**, 094107 (2015).
- [62] M. Hellgren, J. Baima, R. Bianco, M. Calandra, F. Mauri, and L. Wirtz, *Phys. Rev. Lett.* **119**, 176401 (2017).
- [63] M. Hellgren, L. Bague, M. Calandra, F. Mauri, and L. Wirtz, *Phys. Rev. B* **103**, 075101 (2021).
- [64] P. Giannozzi, O. Andreussi, T. Brumme, O. Bunau, M. B. Nardelli, M. Calandra, R. Car, C. Cavazzoni, D. Ceresoli, M. Cococcioni *et al.*, *J. Phys.: Condens. Matter* **29**, 465901 (2017).
- [65] A. Dal Corso, *Comput. Mater. Sci.* **95**, 337 (2014).
- [66] J. Klimeš, D. R. Bowler, and A. Michaelides, *J. Phys.: Condens. Matter* **22**, 022201 (2010).
- [67] S. Baroni, S. de Gironcoli, A. Dal Corso, and P. Giannozzi, *Rev. Mod. Phys.* **73**, 515 (2001).
- [68] H. T. Stokes, B. J. Campbell, and D. M. Hatch, ISOTROPY software suite, iso.byu.edu.
- [69] A. V. Krukau, O. A. Vydrov, A. F. Izmaylov, and G. E. Scuseria, *J. Chem. Phys.* **125**, 224106 (2006).

- [70] S. Grimme, *J. Comput. Chem.* **27**, 1787 (2006).
- [71] G. Kresse and J. Furthmüller, *Phys. Rev. B* **54**, 11169 (1996).
- [72] H. T. Stokes and D. M. Hatch, *J. Appl. Crystallogr.* **38**, 237 (2005).
- [73] D. Orobengoa, C. Capillas, M. I. Aroyo, and J. M. Perez-Mato, *J. Appl. Crystallogr.* **42**, 820 (2009).
- [74] A. Togo and I. Tanaka, [arXiv:1808.01590](https://arxiv.org/abs/1808.01590).
- [75] A. Togo and I. Tanaka, *Scr. Mater.* **108**, 1 (2015).
- [76] S. Sugai, K. Murase, S. Uchida, and S. Tanaka, *Solid State Commun.* **35**, 433 (1980).
- [77] J. A. Holy, K. C. Woo, M. V. Klein, and F. C. Brown, *Phys. Rev. B* **16**, 3628 (1977).
- [78] V. Olevano, M. Cazzaniga, M. Ferri, L. Caramella, and G. Onida, *Phys. Rev. Lett.* **112**, 049701 (2014).